2004:67

LICENTIATE THESIS

Development of a Novel Zeolite Coated ATR-FTIR Sensor

Mattias Grahn

Luleå University of Technology
Department of Chemical Engineering and Geosciences, Division of Chemical Technology

2004:67 | ISSN: 1402-1757 | ISRN: LTU-LIC -- 04/67 -- SE

Development of a Novel Zeolite Coated ATR-FTIR Sensor

Mattias Grahn

November 2004

Luleå University of Technology

Department of Chemical Engineering and Geosciences

Division of Chemical Technology

Abstract

Thin zeolite films have great potential in several novel application areas such as: structured catalysts, membranes and sensors. To fully exploit the advantages of these films it is of great importance to determine the properties of the films. A powerful technique for studies of phenomena at surfaces or in thin films is FTIR/ATR-spectroscopy (Fourier Transform Infra Red / Attenuated Total Reflection). Furthermore, thin zeolite films may be utilized for enhanced selectivity and sensitivity for this technique.
In this work films with a thickness of 200 nm of the zeolites ZSM-5 and silicalite-1 were grown on ZnSe, ZnS, ZrO_2, Si and Ge ATR elements using a method that had been developed previously.

The coated elements were evaluated in a gas sensor application by comparing the sensitivity for a hydrocarbon of zeolite-coated elements versus a standard 10 cm gas cell. The sensitivity was approximately 85 times higher for the coated elements compared to the gas cell at low hydrocarbon concentration. The response time was investigated by exposing the coated element to a step increase of an analyte and recording the response as a function of time. The response was relatively fast, equilibrium was achieved after approximately 250 s, but already after a few seconds a strong signal could be detected.

The coated elements were also used to determine single gas adsorption isotherms. The systems studied were n-hexane/silicalite-1 and p-xylene/silicalite-1. Adsorption isotherms determined at varying temperatures were typical for microporous materials. Capillary condensation was observed at higher concentration of the adsorbate. Henry constants and heats of adsorption determined from low-pressure data agreed well with previously reported data in the literature.

Keywords: Silicalite-1, adsorption, sensor, zeolite, FTIR, ATR

Acknowledgements

First of all, I would like to thank my supervisor, Associate Professor Jonas Hedlund for your guidance during this work and for your constant enthusiasm. Further, I would like to thank Associate Professor Allan Holmgren who has been my assistant supervisor, for his support and helpful discussions regarding spectroscopy. I would also like to thank Prof. Johan Sterte for giving me the opportunity to work within this research group.

I thank Dr. Margareta L. Larsson for teaching me how to run the spectrometer and getting me started with this work. I am also grateful to Dr. Zheng Wang for a fruitful collaboration within this project. Further I would like to thank all the friends and colleagues at the Department of Chemical Engineering and Geosciences with special thanks to Dr. Fredrik Jareman for his computer support during these years.

The Swedish Research Council (VR) is gratefully acknowledged for its financial support.

I would like to give my warmest thanks to my parents and my brother for your support and encouragement. Finally, I wish to thank my girlfriend Johanna for always supporting me and for having such patience with me. I love you!

Mattias Grahn,
Luleå, November 2004.

List of Papers

This thesis is based on the work reported in the following papers, referred to in the text by Roman numerals.

I **Zeolite coated ATR crystals for new applications in FTIR-ATR spectroscopy**
Zheng Wang, Margareta L.Larsson, Mattias Grahn, Allan Holmgren and Jonas Hedlund
Accepted for publication in Chemical Communications.

II **Zeolite coated ATR crystals in FTIR spectroscopy**
Zheng Wang, Mattias Grahn, Margareta L.Larsson, Allan Holmgren and Jonas Hedlund
Submitted to Chemistry of Materials

III **Silicalite-1 coated ATR elements as sensitive chemical sensors**
Mattias Grahn, Zheng Wang, Margareta L.Larsson, Allan Holmgren and Jonas Hedlund
Submitted to Microporous and Mesoporous Materials

IV **Adsorption of n-hexane and p-xylene in thin silicalite-1 films studied by FTIR/ATR spectroscopy**
Mattias Grahn, Allan Holmgren and Jonas Hedlund
Manuscript

Contents

Introduction

Zeolites and zeolite films

Zeolites are a group of minerals of great scientific and industrial importance. The first zeolite mineral was discovered in the middle of the 18th century by the Swedish mineralogist A. Cronstedt. Cronstedt found that the mineral lost water rapidly upon heating, thus seeming to boil. The name zeolite stems from the greek words zeo (to boil) and lithos (stone).

Zeolites are crystalline, hydrated aluminosilicates consisting of a three-dimensional network of $[SiO_4]^{4-}$ and$[AlO_4]^{5-}$ tetrahedra. The tetrahedra are linked by sharing oxygen atoms. More than 150 different zeolite and zeolite-like frameworks are known today, both natural and synthetic [1].
A general formula for zeolite structures can be written as:

$$M_{x/n}[(AlO_2)_x(SiO_2)_y]\cdot wH_2O$$

In the above formula, M is the cation of valence n and w is the number of water molecules. The charge balancing cation is usually a metal cation, ammonium- or alkylammonium cation. If the zeolite contains charge balancing metallic cations these are exchangeable resulting in ion-exchange capacity. Zeolites are therefore used in large quantities as softeners in detergents. The ratio y/x is the important silicon to aluminum ratio, this ratio is always ≥ 1. Some of the physical and chemical properties of the zeolite are determined from the aluminum content in the zeolite; more aluminum in the framework gives a more hydrophilic zeolite.

An important feature of the zeolites originating from the inherent structure is the well-defined pore systems, see Figure 1.

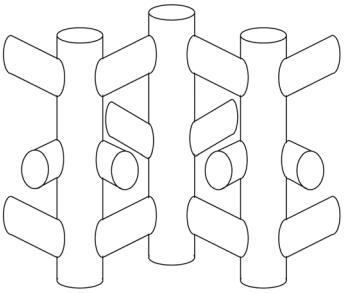

Figure 1. Schematic figure of the MFI channel system.

Pores are classified in three categories according to IUPAC [2]:

- Micopores $d < 2$ nm
- Mesopores $2 < d < 50$ nm
- Macropores $d > 50$ nm

The one-, two or three-dimensional pore system is determined by the crystal structure of the zeolite. The pores may have tubular shape or contain periodic cavities and may be straight or zig-zag. The pore diameters in known zeolites are between 3 and 13 Å, which results in high specific surface area, several hundreds square meters per gram are common. Due to the small pore diameter, vapours condense readily in zeolites. The phenomenon of capillary condensation will be dealt with more thoroughly in a later section. The small and well-defined pore openings of the zeolites results in molecular sieving properties. Molecular sieves are materials that are able to discriminate between different molecules based on size or shape. Small molecules are allowed to enter the pore structure while molecules larger than the pore openings cannot enter.

If the charge balancing cation is substituted for a proton, the acid form of the zeolite is obtained. The acid form of zeolites is commonly used as acid catalysts in various chemical processes.

Acidity in combination with a well-defined pore structure makes zeolites very useful as catalysts. The well-defined pore systems results in selective reactions, which is very desirable.

In this work, thin films of the zeolites ZSM-5 and silicalite-1 were used. Silicalite-1 is strictly speaking not a zeolite since it contains no (or very little) aluminum, it is the pure silica analogue of the zeolite ZSM-5, both having the MFI framework. The absence of aluminum in the framework of silicalite-1 makes it more hydrophobic than its zeolite analogue.

The MFI framework has two types of pores; straight with pore openings of 0.53 x 0.56 nm and zig-zag with pore openings of 0.51 x 0.55 nm.

Thin films of zeolites or zeolite-like materials have been given much attention due to the large potential in the following applications:

- Membranes
- Sensors
- Catalysts

In membrane applications, a thin, defect free film is desirable. The thinner the film the smaller the mass transport resistance, and obviously a defect free film is necessary to obtain as high selectivity as possible [3, 4]. In catalysis, the product composition is dependent on the film thickness, controlling the film thickness could then alter the product composition [5]. Zeolites in sensor applications may be beneficial for selectivity and sensitivity and thin films assure a fast response time of the sensor [6-8].

Zeolite films are most often grown on some kind of support for mechanical strength, although non-supported films also have been reported in the literature [9, 10]. Several methods for preparing zeolite films have been developed. The seed film method was developed at our division [11-13]. In this method, the surface of the support is first positively charged by adsorbing a cationic polymer. Negatively charged colloidal zeolite seed crystals are subsequently electrostatically adsorbed to the charged surface. Finally, the seeded support is placed in a synthesis solution to grow the seed crystals into a continuous film. An organic structure directing agent, or template molecule, is added to the synthesis solution in order to facilitate growth of the zeolite. The template molecule is incorporated in the zeolite pores after synthesis and is often removed by calcination at high temperature, for instance 500ºC, after synthesis.

Defects in films

In most applications it is desirable to reduce the amount of defects in the film to a minimum to obtain a high selectivity. However, in catalysis and sorption applications, defects may be desirable since they may provide alternative diffusion paths, increasing average diffusivity in the film. Knudsen diffusivity in defects in the form of mesopores is several orders of magnitude larger than diffusivity in zeolite pores [14]. Defects are usually classified as pinholes, cracks and open grain boundaries. Pinholes are believed to be a result of incomplete seeding or insufficient film thickness and may occur at certain growth conditions [15, 16]. Several reports on crack formation in zeolite films are available [17-19].

Cracks may form during calcination of the film, most likely due to that the unit cell in MFI zeolite shrinks during template removal [19].

It is likely that some grain boundaries remain "open" after synthesis of the zeolite film. In this case, "open" has the meaning "pathway with a width exceeding the diameter of the zeolite pores. Since zeolite pores are so narrow, "open" may mean that the opening is about a nanometer wide. It may be impossible to close grain boundaries completely, since building blocks during zeolite crystallisation have a certain size [20].

Adsorption

When a clean solid surface is exposed to a gas, some of the gas molecules will adsorb to the surface, which is referred to as the adsorbent and the adsorbed gas is referred to as the adsorbate. The adsorbed amount depends on the pressure of the adsorbate, the temperature and the properties of the adsorbent.

The phenomenon of adsorption plays an important role in both heterogeneous catalysis and in adsorption and membrane applications. Two main types of adsorption processes exists; *chemical* adsorption and *physical* adsorption. Chemical adsorption is also referred to as *chemisorption*.
Chemisorption involves the creation of bonds between the adsorbent and the adsorbate and resembles chemical reactions. Most of the reactions being catalysed by a solid are believed to involve an intermediate step with chemisorption of at least one of the reactants.

Physical adsorption is caused by weak intermolecular forces such as van der Waal, induced dipoles and dipole-dipole interactions. Physical

adsorption resembles condensation of vapours rather than actual chemical reactions as in chemisorption. Physical adsorption is the main phenomenon used in adsorptive separation processes. Further, physical adsorption is used to determine the specific surface area as well as pore sizes and pore size distributions of the adsorbent.

Chemical bonds involving chemical reactions are stronger than the ones involving van der Waal forces. The heat of adsorption is a direct measure of the bond strength between the surface and the adsorbate. This parameter will yield information on which adsorption process is taking place. For physical adsorption the heat of adsorption is approximately 2-3 times smaller than the heat of vaporization [21]. Physical adsorption from gas phase is always an exothermic process.

Usually physical adsorption is very rapid since it does not require activation energy. However, in microporous materials, like zeolites, the uptake may be determined by the rate of diffusion of the adsorbate within the pore system of the adsorbent.

Physical adsorption is an equilibrium process, which is fully reversible. Equilibrium is quickly achieved unless the process is restricted by slow diffusion of the adsorbate.

Physical adsorption is usually nonspecific in contrast to chemisorption, which is highly specific taking place on certain specific sites on the surface. As a consequence chemisorption is restricted to forming a monolayer, whilst in physical adsorption both monolayers as well as multilayers may form. At low partial pressures monolayer adsorption is dominating whilst at higher partial pressures multilayers may form.

Adsorption isotherms

Adsorption isotherms are usually classified according to Brunauer [22], see Figure 2. Microporous materials usually shows type I behaviour. The type I isotherm is also referred to as a Langmuir type of isotherm, with a steep increase in surface coverage at low partial pressures. At higher partial pressures the isotherms starts to level off towards a distinct saturation limit when the pore system is completely filled with the adsorbate. Type II isotherms represent multilayer adsorption on non-porous solids. Type IV isotherms are typical for porous materials containing mesopores where capillary condensation occurs in the mesopores. Types III and V are rare and occurs in systems where the forces of adsorption are relatively weak.

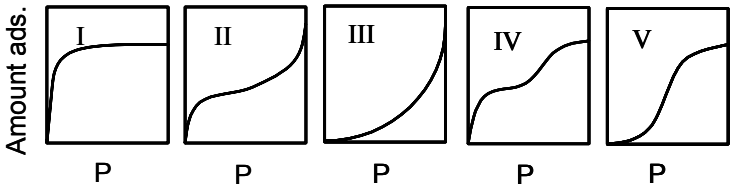

Figure 2. Brunauer's five types of adsorption isotherms.

At low partial pressures of the adsorbate there will be a low surface coverage, and the adsorbed molecules may be regarded as isolated from the neighbours. Assuming that the surface is uniform, the relationship between the partial pressure and the amount adsorbed on the surface will be linear. This relationship is often referred to as Henry's law because of the similarity to the limiting behaviour of gases dissolved in liquids. For a Henry constant expressed in pressure the Henry law is written as:

$$q = K_H P \qquad (1)$$

The loading of the adsorbate is q (mol kg^{-1}), K_H is the Henry constant (mol kg^{-1} Pa^{-1}) and P is the partial pressure of the adsorbate in gas phase.
At higher partial pressures molecules adsorbed at adjoining sites will interact with each other. The surface will begin to reach monolayer coverage alt. in zeolites the micropores will be completely filled. These factors will affect the amount adsorbed so that the linear relationship between the partial pressure and the surface coverage according to equation (1) is no longer valid. To model this behavior a number of adsorption models have been

proposed, a common model is the so-called Langmuir model or the Langmuir isotherm.
When deriving the Langmuir isotherm some assumptions are made:

- Molecules are adsorbed at a fixed number of well-defined localized sites.
- Each site can hold one adsorbate molecule
- The heat of adsorption is independent of surface coverage

The last assumption implies that (1) all sites are energetically equivalent and (2) there is no interaction between molecules adsorbed at adjoining sites.
The last assumption have been subjected to much criticism since (a) most surface are heterogeneous giving rise to energetically different sites and (b) at high surface coverage the molecules will in most cases be so closely packed so that interaction occurs between adjoining adsorbed molecules.
Despite the criticism, the Langmuir model has proved to describe numerous adsorption systems including adsorption in zeolites [23-25].

The Langmuir isotherm can easily be derived by assuming that the rate of adsorption is proportional to the rate of molecular collisions with vacant sites:

$$\textit{Rate of adsorption} = k_A P(1-\Theta) \qquad (2)$$

In the expression, k_A is the adsorption constant, P is the partial pressure of the adsorbate. Further, if q_s is the saturation capacity of the surface and by letting Θ be the fractional surface coverage, q/q_s, this implies that $1-\Theta$ is the fraction of vacant sites.

$$\textit{Rate of desorption} = k_D\Theta \qquad (3)$$

In the expression, is the desorption constant is denoted k_D. At equilibrium the rate of adsorption and desorption are equal, so that

$$k_A P(1-\Theta) = k_D\Theta \qquad (4)$$

By setting $b = k_A/k_D$ and by solving for Θ the following expression is obtained:

$$\Theta = \frac{q}{q_s} = \frac{bP}{1+bP} \tag{5}$$

At high partial pressures $q \rightarrow q_s$ and $\Theta \rightarrow 1$ while at low partial pressures $bP << 1$ and:

$$\lim_{p \rightarrow 0}\left(\frac{q}{P}\right) = bq_s = K_H \tag{6}$$

As a consequence, at low partial pressures, Henry's law is valid. The adsorption equilibrium constant, b, is easily obtained from experimental data. Equation (5) is linearised to:

$$\frac{P}{q} = \frac{P}{q_s} + \frac{1}{q_s b} \tag{7}$$

A plot of P/q as a function of P should yield a straight line with slope equal to $1/q_s$ and the intercept with the y-axis equal to $1/(q_s b)$.

The adsorption equilibrium constant is only constant at constant temperature and can be analysed via the Arrhenius relationship:

$$b = e^{\Delta S_{ads}/R} e^{-(\Delta H_{ads}/RT)} \tag{8}$$

In the equation, ΔS_{ads} is the limiting entropy of adsorption and ΔH_{ads} is the limiting heat of adsorption. Moreover R is the gas constant and T is the temperature. When the temperature is increased b will decrease, since adsorption from gas phase always is an exothermic process.

The isosteric heat of adsorption can be determined from experimental data by measuring isotherms at varying temperatures and using the van't Hoff equation:

$$-\left(\frac{\partial \ln K_H}{\partial T}\right)_q = \left(\frac{\partial \ln P}{\partial T}\right)_q = \frac{-\Delta H_{ads}}{RT^2} \qquad (9)$$

By using $d(1/T)dT = -1/T^2$, equation (9) can be rearranged to

$$\left(\frac{\partial \ln K_H}{\partial (1/T)}\right)_q = \frac{\Delta H_{ads}}{R} \qquad (10)$$

Plotting ln P as a function of $1/T$ would yield a straight line with slope $\Delta H_{ads}/R$ from which ΔH_{ads} can be determined.

Capillary condensation

Adsorption in zeolite films may be affected by capillary condensation in defects (micro, meso and macropores) in the film. For mesoporous defects the radius of a pore in which capillary condensation occurs is given by the Kelvin equation [26].

$$r = \frac{-2\gamma V_m}{RT \ln\left(P/P_0\right)} \qquad (11)$$

The radius is denoted r, γ is the surface tension of the condensing liquid, V_m, is the molar volume of the liquid and P/P_0 is the relative pressure of the condensable vapour. The condensed liquid is assumed to have a continuous surface. However, this is not the case in small pores (micropores) where the size of the adsorbate is of approximately the same size as the diameter of the pores.

In that case a modified version of the Horváth-Kawazoe equation [27, 28] valid for slit shaped pores, may be used:

$$RT \ln\left(\frac{P}{P_0}\right) = \frac{\Delta H_{ads}}{(d-d_0)}\left[\frac{\sigma^{10}}{9d_0^9} - \frac{\sigma^4}{3d_0^3} - \frac{\sigma^{10}}{9(2d-d_0)^9} + \frac{\sigma^4}{3(2d-d_0)^3}\right] \quad (12)$$

In the equation above, d is the slit pore half width. Moreover, σ is the distance between the wall and the adsorbate where the interaction energy equals zero and is defined as:

$$\sigma = \left(\frac{2}{5}\right)^{1/6} \frac{d_A + d_S}{2} = \left(\frac{2}{5}\right)^{1/6} d_0 \quad (13)$$

The critical diameter of the adsorbate molecule is denoted d_A. Further, d_s is the diameter of the adsorbent. The following values were used in this work:

- d_A(n-hexane): 0.43 nm [29]
- d_A(p-xylene): 0.585 nm [30]
- d_S: 0.276 nm [31]

The width of the defect, d_i, is related to the slit pore half width by the relationship, $d_i = 2d - d_S$.

FTIR/ATR spectroscopy

Infrared spectroscopy

FTIR (Fourier Transform Infra Red) spectroscopy is a technique where electromagnetic radiation in the infrared region interacts with oscillating dipoles in a sample, resulting in an absorption spectrum. The vibrational

spectra of different groups in a molecule act as fingerprints, making it possible to identify molecules in a mixture using FTIR spectroscopy.

The vibration modes may be stretching- or bending vibrations. In stretching vibrations there is a change in the length of the bond, and the change may be symmetric or asymmetric. Bending vibrations are sometimes also referred to as deformation vibrations and involve a change in the bond angles. Different types of deformations can occur such as; wagging, rocking, scissoring and twisting.

For a vibration being infrared active, i.e. the vibration absorbs infrared radiation, the dipole moment of the molecule must change during the molecular vibration. The bonds vibrate at specific frequencies depending on the masses of the atoms connected by the bonds. The frequency is usually expressed in wavenumbers (cm^{-1}).

To determine the relationship between the radiation absorbed by the sample and the sample concentration Beer's law is often used:

$$A = \log \frac{I_0}{I} = \varepsilon bc \qquad (14)$$

A is the absorbance, I_0 is the intensity of the incident and I is the intensity of the radiation leaving the sample. Further, ε is the absorptivity, a mode specific frequency dependent parameter, b is the sample thickness and c is the sample concentration. The *spectrum* of a sample is the absorbance recorded as a function of the wavenumber.

The ATR technique

Infrared spectra can be recorded using several experimental techniques such as transmission, diffuse reflectance, infrared microspectroscopy etc [32].

A technique specially suited for studying processes at surfaces and in thin films is the ATR (Attenuated Total Reflection) technique [33, 34]. Ninnes et al., Lu et al. and Han et al. [35-37] studied and reported the adsorption of hydrocarbons from aqueous solution whilst Chittur [38] reported adsorption of proteins. Göbel et al. [39] have used the ATR technique to study the diffusion of chlorinated hydrocarbons in thin polymer membranes. Wolf et al. and Süer et al. [40, 41] both used the ATR technique for in-situ reaction monitoring. In Süer's case, an uncoated cylindrical ATR element was placed in the center of a packed bed reactor for studying n-heptane cracking over a commercial Y-type zeolite.

In the ATR technique the infrared beam is internally reflected in a waveguide, see Figure 3. The technique is based on the total reflection of electromagnetic radiation in the interface between two media having different refractive indices.

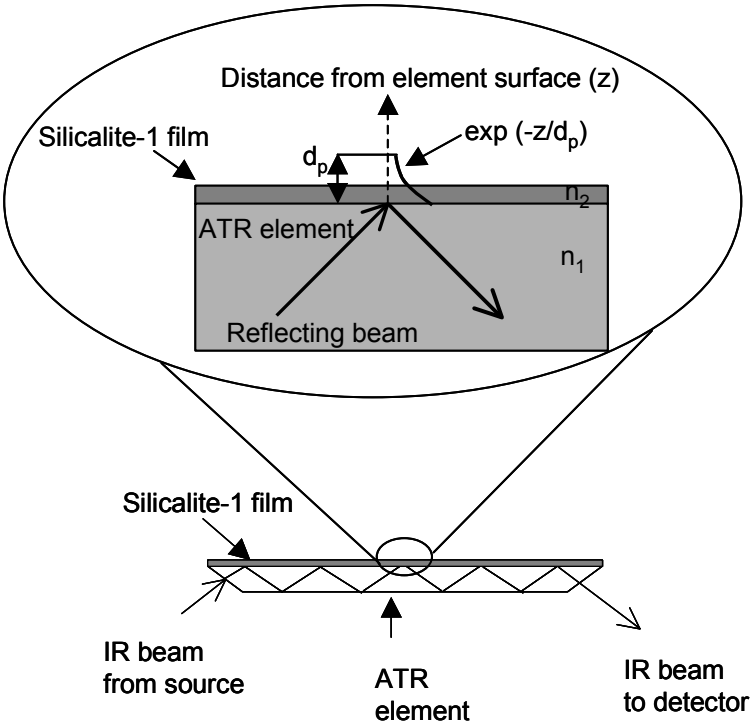

Figure 3. Schematic picture of the ATR principle.

A necessary condition for total internal reflection is that the angle of incidence is larger than the critical angle, $\alpha_{crit} = \sin^{-1} n_{21}$, where $n_{21} = \frac{n_2}{n_1}$ is the ratio of the rarer mediums refractive index divided by the denser mediums refractive index. At each reflection an evanescent wave is created extending beyond the reflecting media, see Figure 3. This evanescent wave has the same frequency as the IR beam from the source and can interact with molecules in the vicinity of the interface. The intensity of the wave decreases exponentially with distance from the waveguide, usually the effective penetration depth is less than a wavelength. The rapid decrease in intensity of the wave with distance from the waveguide makes the technique especially suited for studying surface phenomena, since only molecules in

the vicinity of the surface will be detected. Multiple reflection waveguides, as in Figure 3, are often used for enhanced sensitivity.

The depth of penetration is defined as the distance normal to the waveguide where the intensity of the electric field is e^{-1} of that at the surface of the waveguide and is given by:

$$d_p = \frac{\lambda_1}{2\pi\left(\sin^2\alpha - \left(\frac{n_2}{n_1}\right)^2\right)^{1/2}} \qquad (15)$$

The penetration depth is denoted d_p, $\lambda_1=\lambda/n_1$ is the wavelength of the IR-radiation in the denser medium with refractive index n_1, α is the angle of incidence of the radiation and n_2 is the refractive index of the less dense medium. The wavelength dependence of the penetration depth implies that ATR spectra and transmission spectra of the same molecule will not be identical. In ATR spectroscopy, the radiation with long wavelength will penetrate deeper into the sample than radiation with short wavelength, causing the bands at longer wavelengths to be more intense than the ones at shorter wavelength.

Scope of the present work

Adsorption, diffusion and reactions are important processes taking place within zeolites. Although much effort has been devoted to gain a deeper understanding about these processes, there is still a lack of knowledge, especially within the fields of multi-component- adsorption, diffusion and reactions in zeolites.

The present work aims at evaluating ATR elements coated with well defined, thin zeolite films as a tool for studying the processes taking place in zeolites, as well as investigating the films in sensor applications.

Experimental

Film synthesis

Trapezoidal ATR elements of ZnS, Ge, ZnSe and ZrO_2 (50x20x2 mm) and Si (50x20x1 mm) having 45º cut edges were used in this study. Some of the material properties for the elements are reported in Table 1.

Table 1. Properties of the ATR elements.

Material	Refractive index at 1000 cm^{-1} (n)	Melting point (ºC)	Spectral range (cm^{-1})
ZnSe	2.4	1520	20000-650
ZnS	2.2	1830	17000-950
ZrO_2	2.4	2700	25000-1800
Si	3.4	1420	9500-950
Ge	4.0	936	5500-870

In order to obtain a free path for the IR beam entering and leaving the ATR element the cut edges of the element were protected in order to prevent zeolite growth on these surfaces. This was achieved by coating the surfaces with an epoxy polymer. To obtain a surface suitable for seeding the elements were cleaned. The ZnS, ZnSe and ZrO_2 elements were immersed in acetone and treated in an ultrasonic bath for ten minutes and subsequently rinsed with distilled water. An alternative procedure was used for the Si elements. The Si elements were first treated in the same way as the ZnS elements, followed by five minutes of boiling in a solution having the volume composition $5H_2O$: $1H_2O_2$: $1NH_3$, and then boiled another five minutes in a solution having a volume composition of $6H_2O$: $1H_2O_2$: 1HCl. Finally, the elements were rinsed in distilled water. The Ge element was treated differently. The element was first treated in the same way as the ZnS

elementsand then dipped in a 38 wt% HF solution for 5-10 s and washed with distilled water. The element was subsequently dipped in a 27 wt% H_2O_2 solution for 10- 15 s and then rinsed in distilled water. These two procedures were repeated four times to remove several atom layers of Ge. Finally, the element was oxidized by dipping the element in a 27 wt% H_2O_2 solution for 10-15 seconds.

To render the surface of the elements positively charged the elements were treated in a 0.4 wt-% solution of a cationic polymer for five minutes. To remove excess polymer the elements were rinsed with a 0.1 M ammonia solution. Subsequently, the charged reversed elements were immersed in a sol containing 60 nm silicalite-1 seeds. Finally, the seeds were grown into a continuous, polycrystalline silicalite-1 film by hydrothermal treatment at 100ºC for 24 h using a synthesis solution with molar composition 3TPAOH: $25SiO_2$: $1450H_2O$: 100EtOH. Following film growth, the elements were rinsed with a 0.1 M ammonia solution and then dried in an oven at 50ºC.
The TPA molecules used as template molecules and the protective polymer used were removed by calcination at 500ºC.

Instrumentation

To determine the film thickness and the surface morphology a Philips XL 30 Scanning Electron Microscope (SEM) equipped with a LaB_6 emission source was used. To collect X-ray diffraction patterns a Siemens D5000 powder X-ray diffractometer (XRD) was used. All infrared spectra were recorded using a Bruker IFS113V spectrometer equipped with a mercury cadmium telluride (MCT) detector. The cells (see below) were mounted at a vertical ATR accessory supplied by Spectratech.

Two different types of cells were manufactured. In the work reported in Paper I and II a simple stainless steel flow cell was used, see Figure 4. The cell was sealed using a viton o-ring and the gas was supplied via tubing through the lid of the spectrometer.

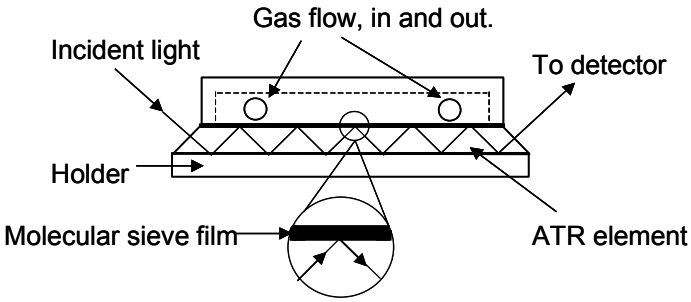

Figure 4. Schematic figure of the non-heatable flow cell.

In the work reported in Paper III & IV, a heatable flow cell was used allowing in-situ drying of the film as well as measurements at elevated temperatures. The cell was manufactured from stainless steel and sealed with graphite gaskets, see Figure 5. Stainless steel tubing through the wall of the sample compartment was used for supplying gas to the cell. Heating cartridges were used for heating the cell and the temperature was measured and controlled via a thermocouple connected to a programmable temperature controller.

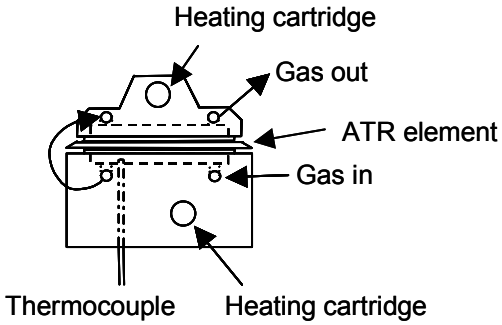

Figure 5. Schematic figure of the heatable flow cell.

Experimental set-up

To vary the composition of the feed to the cells a gas delivery system was constructed, see Figure 6. The system consists of three mass flow controllers (MFC's) having different flow ranges and two saturators connected in series to ensure saturation of the gas stream. The first saturator was held at room temperature whilst the latter saturator was fitted with a cooling jacket connected to a circuit of thermostated cooling water. Usually, one of the mass flow controllers was used for controlling the flow of the carrier gas to the saturators, whilst one of the others was used for dilution of the flow from the saturators to the desired partial pressure of the hydrocarbon.

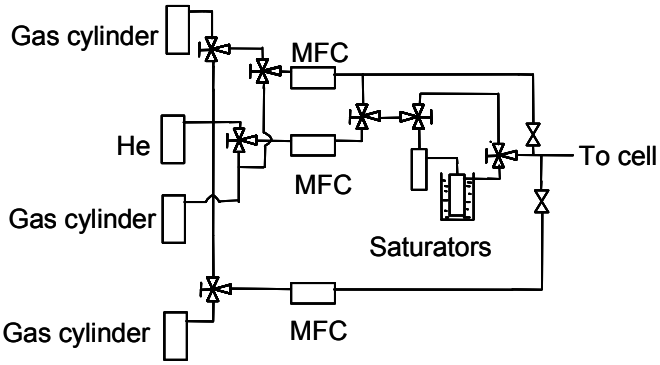

Figure 6. Schematic figure of the gas delivery system.

A typical adsorption measurement was performed as follows. The film was first dried. When the simpler cell was used, the films were dried by placing the ATR element in a beaker flushed with dry argon and the beaker was heated to 250ºC for at least 12 h. The element was then mounted in the cell under a flow of dry argon or nitrogen. When the heatable cell was used the film was dried in-situ at 260ºC under a feed of pure helium for 12 h. After drying, the cell was mounted in the spectrometer and a background spectrum was recorded by averaging 500 scans with a feed of pure helium to the cell. After recording the background the feed was changed to helium containing a hydrocarbon. At equilibrium, a spectrum was recorded. Each spectrum was averaged over 250 scans.

Results

General characterization of the films (Paper I and II)

Continuous thin ZSM-5 and silicalite-1 films were successfully grown on Zinc Sulphide (ZnS), Zirconia (ZrO_2), Silicon (Si) and Germanium (Ge) ATR elements.

Top (a) and side view (b) SEM images of a silicalite-1 film on a Si substrate are presented in Figure 7. The thickness of the film is approximately 200 nm. The silicalite-1 films on a ZnS substrate appeared very similar.

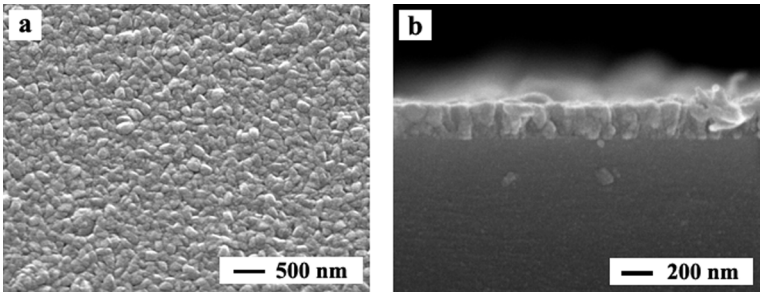

Figure 7. SEM top (a) and side (b) view images of a silicalite-1 film on a Si substrate after 24 hours of hydrothermal treatment at 100ºC.

During synthesis of the films, MFI crystals are formed in the bulk of the synthesis solution. An XRD pattern of purified crystals formed in the bulk is shown in Figure 8 (a), the pattern is typical for randomly oriented silicalite-1 crystals.

The XRD pattern of a silicalite-1 coated ZnS substrate is shown in Figure 8 (b), the reflection labeled with a star stems from the ZnS substrate. It can be concluded that the film consists of MFI crystals. XRD pattern of silicalite-1 films on Si substrates were very similar.

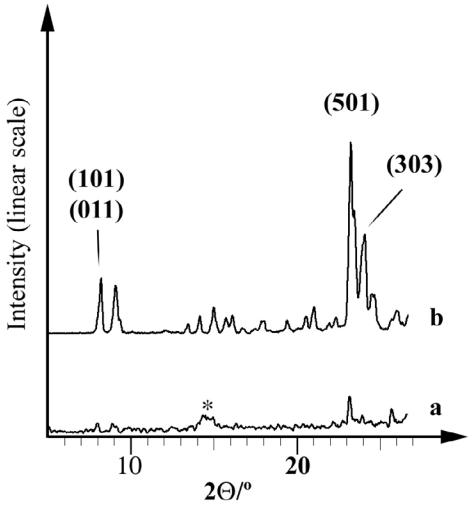

Figure 8. X-ray diffraction patterns of (a) purified bulk product powder, used as reference, and (b) a silicalite-1 film on a ZnS element after 24 hours of hydrothermal treatment at 100ºC. The peak labelled with a star stems from the ZnS substrate.

The films were further characterized using FTIR/ATR – spectroscopy. A spectrum of a silicalite-1 film on a Si ATR element is shown in Figure 9. The spectrum shows some absorption bands in the region 2000-1600 cm^{-1}, which are assigned to overtones of vibrations in the silicalite-1 lattice. Moreover, a band is observed at 3743 cm^{-1}, which is a typical band for terminal SiOH - groups in silicalite-1.

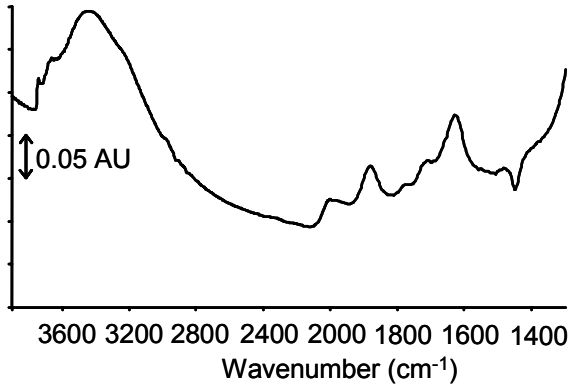

Figure 9. IR spectrum of a silicalite-1 film on a Si element.

Films on ZnSe were damaged and discontinuous, probably due to oxidation of the elements to ZnO during calcination, as supported by the appearance of ZnO reflections in the XRD pattern.

Sensitivity of a silicalite-1 coated ATR element compared to an uncoated element (Paper III)

The sensitivity of a silicalite-1 coated ZnS element for the detection of n-hexane in gas phase was compared to an uncoated element. The absorbance from the coated element was compared with the absorbance obtained from the uncoated element. The experiments were carried out at room temperature and the elements were exposed on both sides to a gas mixture of n-hexane in helium with a relative pressure of n-hexane of $6*10^{-5}$. Figure 10 presents the C-H stretching region of the two spectra.

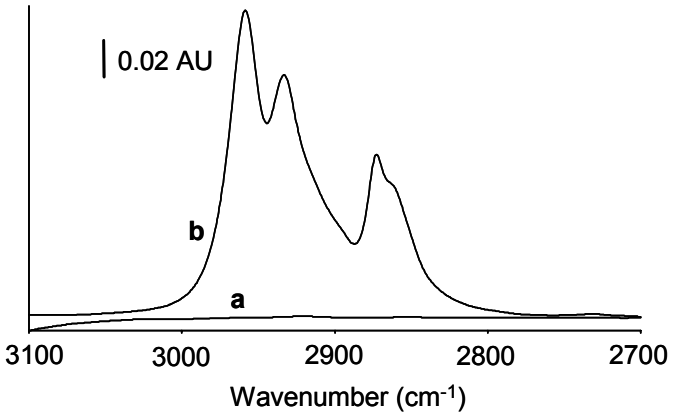

Figure 10. IR spectra of n-hexane using an uncoated ZnS element (a) and a silicalite-1 coated element (b). The experiment was performed at room temperature with a n-hexane content in the feed of 0.006 % of saturation.

Spectra were recorded by accumulating 250 scans. The uncoated element (a) showed only weak absorption bands, slightly above noise level, whilst distinct bands were obtained using the coated element (b). The peak height of the 2960 cm^{-1} absorption band was approximately 180 times higher for the coated element.

Sensitivity of a silicalite-1 coated ATR element compared to a gas cell (Paper III)

Experiments were carried out to compare the sensitivity of coated elements with a 10 cm gas cell. The experiments were performed at room temperature using a Si element coated with a silicalite-1 film on one side. The cells were fed with a gas containing n-hexane in helium with a relative pressure of n-hexane corresponding to $6*10^{-5}$. Figure 11 (a) shows the spectrum when a 10 cm gas cell was used and spectrum (b) was recorded using the coated ATR element. The peak height of the 2967 cm^{-1} band was used for comparison. The silicalite-1 coated element has approximately 85 times stronger absorbance.

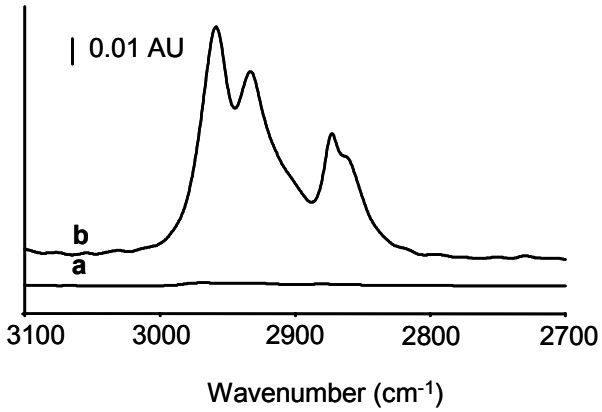

Figure 11. IR spectra of n-hexane recorded using (a) a 10 cm gas cell, and (b) a Si element coated on one side with a silicalite-1 film. The experiment was performed at room temperature with n-hexane content in the feed of 0.006 % of saturation.

Increasing the path length in the gas cell would yield a higher absorbance. On the other hand, several methods could be used for increasing the absorbance in ATR spectroscopy. Coating both sides of the ATR element would yield a stronger absorbance; another method would be to increase the angle of incidence since this would give more reflections inside the waveguide. Further, increasing the film thickness would result in stronger absorbance since more of the analyte would be available for detection by the evanescent field (this option would only be possible up to a certain limit depending on the penetration depth). Using longer and thinner waveguides such as optical fibers would also yield a higher absorbance.

Response time (Paper III)

The response time for the silicalite-1 coated ATR element was also investigated. A ZnS element coated on both sides was used in the experiment. The number of scans was reduced to 10 because of the shorter data acquisition time needed in this experiment. The element was subjected to a step increase of n-hexane from $P/P_0 = 0$ to $P/P_0 = 0.01$ at 27ºC. By following the progression of the 2960 cm^{-1} band the response time was estimated, see Figure 12.

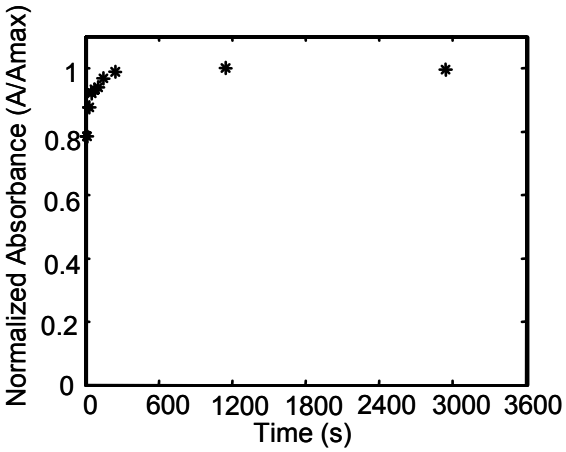

Figure 12. Plot of the normalized absorbance (A/A_{max}) as function of time for the system n-hexane adsorbed in a silicalite-1 film. The experiment was carried out at 27ºC and the absorbance was measured at 2960 cm^{-1}.

It can be concluded that equilibrium is achieved after approximately 250 s, but already at the first point, averaged between approximately t=5 s to t=15 s, the absorbance was 79% of the value at equilibrium, which indicates a relatively fast sensor response time. It is likely that the response time will be even shorter for thinner films, higher temperatures and molecules with higher diffusivity in the adsorbent.

High sensitivity towards hydrocarbons combined with a fast response time and the versatility of FTIR spectroscopy, makes zeolite coated ATR elements a very interesting choice for studying adsorption, diffusion and reactions taking place within the films. The sensor seems ideal for detection of low concentrations of hydrocarbons in gas.

Adsorption isotherms in silicalite-1 (Paper IV)

Single-gas adsorption measurements were carried out in order to evaluate the ATR technique as a tool for studying adsorption processes.

n-Hexane

Adsorption isotherms of n-hexane in silicalite-1 were determined at three temperatures, ranging from 300 K to 308 K, using the heatable flow cell. The isotherms are shown in Figure 13.

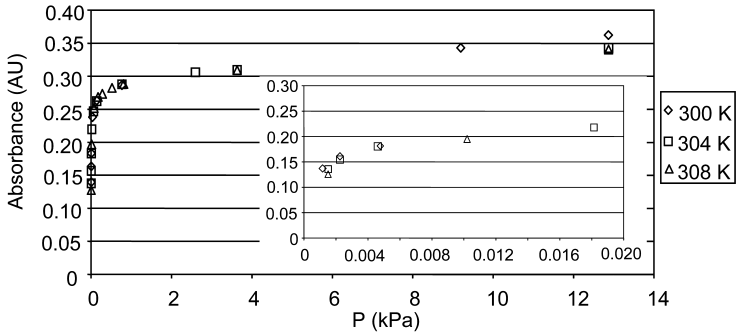

Figure 13. Adsorption isotherms of n-hexane in silicalite-1, the insert shows the low-pressure region.

The isotherms show a fast increase in the surface coverage at low pressures, which is characteristic for microporous materials. At higher pressures the isotherms are not flat as would be expected when the zeolite pore structure is saturated. It seems as mesopores are present in the film, which is in agreement with previously reported findings [42].

The Langmuir plot of the data recorded at 300 K is presented in Figure 14. A curvature is observed, probably originating from capillary condensation in defects at higher pressures.

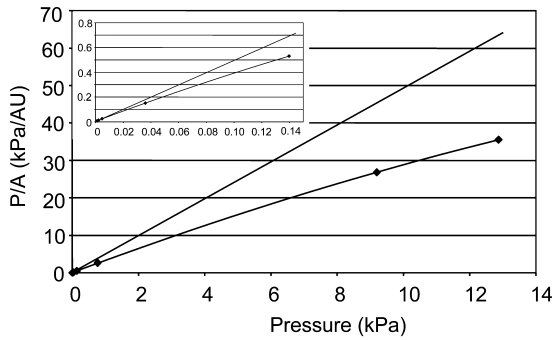

Figure 14. Langmuir plot for the system n-hexane/silicalite-1 at 300 K, the insert shows the low pressure region.

The Henry constant was determined from the tangent of the curve at low pressures, see insert Figure 14. Henry constants determined at each temperature are presented in Table 2 together with literature data for comparison.

Table 2. Henry constants for n-hexane obtained in the present work and literature data.

	Henry constant (mol/(kg Pa))			
Temp. (K)	This work	[43]*	[44]**	[45]***
300	2.8	3.1	0.17	7.0
303		2.35		
304	1.8	2.1	0.12	4.9
308	1.4	1.5	0.08	3.4
373				0.023

* Extrapolated from 303 K using equations (6) and (8).

** Extrapolated using ΔH_{ads} = -70500 J/mol and the relationship $K_H = 9.18 * 10^{-14} * e^{-(\Delta H_{ads}/RT)}$ as reported in the paper.

*** Extrapolated from 373 K using equations (6) and (8).

The Henry constants obtained in this work agrees well with previously reported, although there are some scattering in the data.
The isosteric heat of adsorption was determined from the slope of the plot in Figure 15 to -69 kJ/mol.

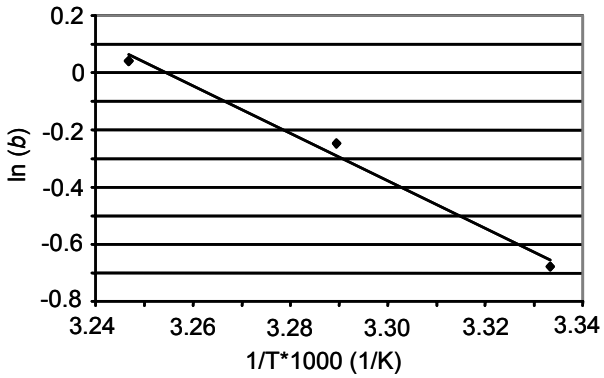

Figure 15. Arrhenius plot for the system n-hexane/silicalite-1.

Heats of adsorption close to -70 kJ/mol have been reported [43-46].

p-Xylene

Adsorption isotherms for p-xylene were determined at 300 and 304 K. The isotherms are presented in Figure 16. Several groups have reported a step in the isotherm for the adsorption of p-xylene in silicalite-1. This step occurs at about half the saturation loading. The isotherm further shows a plateau when the pore system is saturated. The step is absent in the isotherms obtained in this study. Song and Rees [47] has reported that a sample containing a high concentration of internal SiOH groups, indicating defects in the crystal structure, shows a less defined step in a p-xylene isotherm compared to a sample with a low amount of internal SiOH groups. Song and Rees conclude that defects in the silicalite-1 crystals affects the adsorption of hydrocarbons in silicalite-1. Further, the authors speculate that the effect of defects is more pronounced for aromatic – MFI systems than for alkane – MFI systems. The reason for this would be additional interaction between adsorbate and adsorbent in aromatic – MFI systems compared to alkane - MFI systems where only weak dispersion forces are involved.

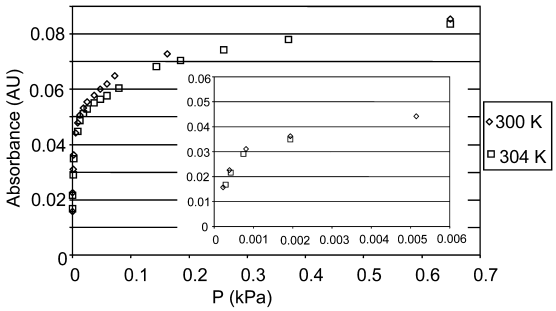

Figure 16. Adsorption isotherms of p-xylene in silicalite-1, the insert shows the low-pressure region.

The Langmuir plot for p-xylene data showed the same curvature as in he case of n-hexane. Henry constants were determined in the same way as for n-hexane, using low-pressure data, the constants are presented in Table 2, together with literature data. The isosteric heat of adsorption was determined to -58 kJ/mol, in agreement with previous reports (-41 to -80 kJ/mol) [48].

Table 3. Henry constants for p-xylene obtained in this work and values found in the literature.

	Henry constant (mol/(kg Pa))			
Temp. (K)	This work	[48] **	[49]	[45]
293	3.7*	8.35		
300	2.8	4.2		
304	2.1	2.9		
313	1.0*	1.3	0.68	0.60

* Extrapolated from 300 K using equations (6) and (8).

** Extrapolated from 293 K using equations (6) and (8).

Conclusions

Silicalite-1 and ZSM-5 films have been successfully grown on waveguides of various crystals for use in ATR spectroscopy. The thicknesses of the films were independent of the substrate.

The coated ATR crystals were very sensitive for hydrocarbons (n-hexane). The sensitivity was also compared with a standard 10 cm gas cell. It was also shown that the response time of the sensor was relatively fast. Adsorption isotherms for n-hexane and p-xylene in silicalite-1 were determined at various temperatures. Henry constants adsorption heats determined from the isotherms at low pressures agreed well with previously reported data. Capillary condensation in defects was observed at higher pressures.

Zeolite coated waveguides in combination with FTIR spectroscopy are extremely promising tools for studying adsorption, diffusion and reaction in zeolites under well defined conditions. The novel sensors show promising sensitivity and response time and are possibly very selective as well.

Future work

Since this is pioneering work on zeolite-coated waveguides, most of the work probably remains. Examples of possible future work are presented below.

- Complete paper IV with data at higher temperature.
- Study reactions catalyzed by the zeolite and possibly identify reaction intermediates.
- Compute defect distribution in the film by comparing isotherms from small (n-hexane) and bulky molecules (triisopropylbenzene).
- Determine orientation of adsorbed molecules in a strongly oriented molecular sieve film using polarized radiation.
- Multi component sorption.
- Diffusion measurements by using rapid-scan or step-scan techniques.
- Detection of very small amounts of organic compounds in water.
- In-situ study of the calcination.

References

[1] C. Baerlocher, W. Meier, D. Olson, Elsevier (2001)
[2] K. Sing, D. Everett, R. Haul, L. Moscou, R. Pierotti, J. Rouquerol, T. Siemieniewska, Pure and Applied Chemistry 57, (1985) 603-619.
[3] J. Hedlund, F. Jareman, M.H. Anthonis, A.J. Bons, J Memb Sci 222, 1-2(2003) 163-179.
[4] Y. Li, S. Huang, S. Wu, X. Yuan, Catalysis Letters 87, 1-2(2003) 31-35.
[5] O.L. Oudshoorn, M. Janissen, W.E.J. van Kooten, J.C. Jansen, H. van Bekkum, C.M. van den Bleek, H.P.A. Calis, Chem Eng Sci 54, 10(1999) 1413-1418.
[6] S. Mintova, T. Bein, Microporous and Mesoporous Materials 50, (2001) 159-166.
[7] M. Vilaseca, J. Coronas, A. Cirera, A. Cornet, J. Morante, J. Santamaría, Catalysis today 82, (2003) 179-185.
[8] J. Zhou, S. Zhang, F. Zhou, Y. Huang, P. Yang, M. Bao, IEEE International Symposium on Applications of Ferroelectrics (2002) 471-474.
[9] V. Tricoli, J. Sefcik, A. McCormick, Langmuir 13, 16(1997) 4193-4196.
[10] Y. Kiyozumi, F. Mizukami, K. Maeda, M. Toba, S. Niwa, Advanced Materials 8, 6(1996) 517-520.
[11] Hedlund J., Schoeman B.J. and Sterte J. , in: Chon H., Ihm S.-K. and Uh Y.S. (Eds.), Progress in Zeolites and Microporous Materials. 105, Elsevier Science, Amsterdam. (1997) pp 2203-2210.
[12] J. Hedlund, B. Schoeman, J. Sterte, Chem Commun (1997) 1193-1194.
[13] J. Hedlund, B. Schoeman, J. Sterte, Int Pat Appl WO 97/33684 (1997)
[14] S. Auerbach, K. Carrado, P. Dutta, ,Handbook of Zeolite Science and Technology, Marcel Dekker Inc., New York, (2003) pp 11.
[15] Jansen J.C., Nugroho W. and van Bekkum H. , in: von Ballmoos R. and et al (Eds.), Proceedings of the 9th International Zeolite Conference. 3, Butterworth-Heinemann, USA. (1993) pp 247-254.

[16] J.C. Jansen, J.H. Koegler, H. van Bekkum, H.P.A. Calis, C.M. van den Bleek, F. Kapteijn, J.A. Moulijn, E.R. Geus, N. van der Puil, Microporous and Mesoporous Materials 21, (1998) 213-226.
[17] M.J. den Exter, H. van Bekkum, C.J.M. Rijn, F. Kapteijn, J.A. Moulijn, H. Schellevis, C.I.N. Beenakker, Zeolites 19, 1(1997) 13-20.
[18] J. Dong, Y.S. Lin, M.Z.-C. Hu, R.A. Peascoe, E.A. Payzant, Microporous and Mesoporous Materials 34, 3(2000) 241-253.
[19] E.R. Geus, H. van Bekkum, Zeolites 15, 4(1995) 333-341.
[20] C. Kirschhock, R. Ravishankar, L. VanLooveren, P. Jacobs, J. Martens, Journal of Physical Chemistry B 103, (1999) 4972-4978.
[21] D. Rutven, ‚Principles of adsorption and adsorption processes, Wiley-Interscience, New York, (1984)
[22] D. Shaw, ‚Introduction to Colloid & Surface Chemistry, Butterworth-Heineman, Oxford, (1992)
[23] H. Tournier, A. Barreau, B. Tavatian, D. Le Roux, J. Moise, J. Bellat, C. Paulin, Industrial and Engineering Chemistry Research 40, (2001) 5983-5990.
[24] G. Gou, Y. Long, Separation and Purification Technology 24, (2001) 507-518.
[25] P. Mathias, R. Kumar, J. Moyer, J. Schork, S. Srinivasan, S. Auvil, O. Talu, Industrial and Engineering Chemistry Research 35, (1996) 2477-2483.
[26] D.D. Do, ‚Adsorption analysis: Equilibria and kinetics, Imperial College Press, London, (1998)
[27] F. Jareman, J. Hedlund, D. Creaser, J. Sterte, Journal of Membrane Science 236, 1-2(2004) 81-89.
[28] G. Horvath, K. Kawazoe, Journal of Chemical Engineering of Japan 16, 6(1983) 470-475.
[29] D. Breck, ‚Zeolite Molecular Sieves, Krieger Publishing Company, Malabar, (1984)
[30] C. Gump, V. Tuan, R. Noble, J. Falconer, Industrial and Engineering Chemistry Research 40, 2(2001) 565-577.
[31] S.U. Rege, R.T. Yang, Aiche J 46, 4(2000) 734-750.
[32] N. Colthup, L. Daly, S. Wiberly, ‚Introduction to Infrared and Raman Spectroscopy, Academic Press, San Diego, (1990)
[33] N. Harrick, ‚Internal Reflection Spectroscopy, John Wiley & Sons, Inc. (1967)
[34] F. Mirabella, ‚Internal Reflection Spectroscopy, Theory and applications, Marcel Dekker, New York, (1993)

[35] B.J. Ninness, D.W. Bousfield, C.P. Tripp, Appl Spectrosc 55, 6(2001) 655-662.
[36] Y. Lu, L. Han, C.J. Brinker, T.M. Niemczyk, G.P. Lopez, Sensors and Actuators B 35-36, (1996) 517-521.
[37] L. Han, T.M. Niemczyk, D.M. Haaland, G.P. Lopez, Appl Spectrosc 53, 4(1999) 381-389.
[38] K. Chittur, Biomaterials 19, (1998) 357-369.
[39] R. Göbel, R.W. Seitz, S.A. Tomellini, R. Krska, R. Kellner, Vibrational Spectroscopy 8, (1995) 141-149.
[40] U. Wolf, R. Leiberich, J. Seeba, Catalysis today 49, (1999) 411-418.
[41] M. Süer, Z. Dardas, Y. Ma, W. Moser, Journal of Catalysis 162, 2(1996) 320-326.
[42] O. Öhrman, V. Msimang, K. Möller, J. Hedlund, microporous and mesoporous materials in press, (2004)
[43] J. Fox, V. Rooy, S. Bates, Microporous and mesoporous materials 69, (2004) 9-18.
[44] M. Sun, O. Talu, D. Shah, J Phys Chem 100, (1996) 17276-17280.
[45] T. Clark, H. Deckman, D. Cox, R. Chance, Journal of Membrane Science 230, (2004) 91-98.
[46] Y. Yang, L. Rees, Microporous materials 12, (1997) 117-122.
[47] L. Song, L.V.C. Rees, Microporous and mesoporous materials 35-36, (2000) 301.
[48] J. Li, O. Talu, Journal of the Chemical Society Faraday Transactions 89, 11(1993) 1683-1687.
[49] R. Richards, L. Rees, Zeolites 8, (1988) 35-39.